Exploration of out-of-plane magnetic textures induced by magnetic field in Co monolayers

Dylan Harris

A senior thesis submitted to the faculty of
Brigham Young University
in partial fulfillment of the requirements for the degree of

Bachelor of Science

Karine Chesnel, Advisor

Department of Physics and Astronomy

Brigham Young University

ABSTRACT

Exploration of out-of-plane magnetic textures induced by magnetic field in Co monolayers

Dylan Harris
Department of Physics and Astronomy, BYU
Bachelor of Science

The performance of magnetic recording devices crucially depends on our knowledge and control of the magnetic textures that may form in the media. To further explore this, we investigate ferromagnetic cobalt (Co) thin films which exhibit interesting textures formed by magnetic domains at the nanoscale. Magnetic domains are regions where the local magnetic moments align in the same direction via exchange couplings. Such regions can extend from about 10 nm to several microns. The direction of magnetization may be out-of-plane (OOP) or in-plane (IP), depending on various parameters including the thickness of the film and the magnitude and direction of an applied magnetic field. Investigating the morphology of magnetic texture via the use of an Atomic/Magnetic Force Microscope (AFM/MFM) allows access to the OOP component of magnetization under a changing magnetic field in-situ. By comparing AFM and MFM images taken at the same location of the sample, we can identify purely magnetic textures that form and change throughout the magnetization process, as an OOP field is applied. We also investigate how these textures correlate to both the IP and OOP magnetization, which we measured using Vibrating Sample Magnetometry (VSM). We found that the magnetic texture is the most contrasted slightly above remanence and fades away with applied field, and reappears differently when the field is released. We also found that this behavior is dependent on Co thickness.

Keywords: Magnetic Domains, Texture, Magnetization, Atomic Force Microscopy, Magnetic Force Microscopy

ACKNOWLEDGMENTS

I would like to thank Dr Chesnel for her help in giving advice and pioneering the project, Kistiaan Tempst for collaboration and the acquisition of the samples, Joey Ray for help with the AFM, Riley Brinkerhoff for showing me how to start, Josh Vawdrey for fixing broken machines, Bridget Kemper for staying with me through it all.

Contents

List of Figures

Chapter 1

Introduction

The following sections provide an introduction to magnetic thin films, with particular emphasis on previous studies of thin films exhibiting perpendicular magnetic anisotropy (PMA). An overview of the present study on single-layer cobalt thin films is also provided.

1.1 Background

The magnetic properties of thin films have been extensively studied because of their importance in both fundamental physics and technological applications. [1] In particular, ferromagnetic thin films have attracted significant interest for their use in magnetic storage technologies. [2] Thin films exhibiting perpendicular magnetic anisotropy (PMA) have received particular attention because they enable substantially higher storage densities in magnetic recording devices such as hard disk drives. Understanding the magnetic behavior of individual ferromagnetic layers provides insight into the fundamental mechanisms governing these systems and may contribute to the optimization of PMA-based devices. PMA is most commonly achieved using multilayer thin films composed of alternating ferromagnetic and nonmagnetic layers. [3] The interfaces between these layers give rise to strong magnetic anisotropy, favoring an out-of-plane alignment of the magnetic moments. [2, 3] Such

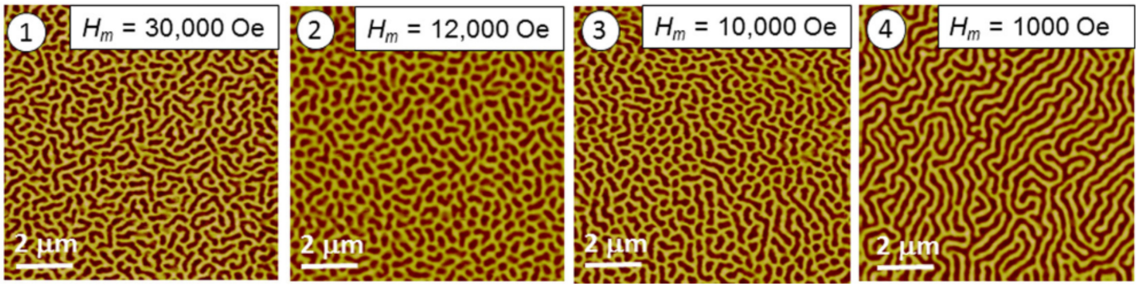

Figure 1.1 Magnetic domains observed at remanence in a Co/Pt multilayer sample following a specific magnetic hysteresis protocol. Extracted from [4]

multilayer structures are widely used in magnetic recording media, including hard disk drives and magnetic tapes. [1] The evolution of magnetic domains under an applied magnetic field is therefore of considerable interest for understanding the behavior of these materials. Compared with multilayer systems, single-layer thin films contain much less magnetic material, making measurements of the local magnetization more challenging. Furthermore, important questions remain regarding the relationship between the microscopic magnetic texture and the macroscopic magnetic response of these films. Magnetic textures arise from the competition between different energy contributions and organize into domains that minimize the total magnetic energy. [4] Depending on the material properties and magnetic history, these domains can exhibit a variety of morphologies, including labyrinthine stripe domains; [5] bubble domains, as illustrated in Fig 1.1; [4] vortices; [4] and skyrmions. [6] Vortices and skyrmions are localized spin textures in which the magnetic moments adopt characteristic rotational configurations. [7] The morphology of these domain patterns evolves significantly with the applied magnetic field and depends strongly on the magnetic history of the sample. [3] Past research on these domain patterns has been performed using a variety of methods, including magnetic force microscopy [8] and electron microscopy. [9]

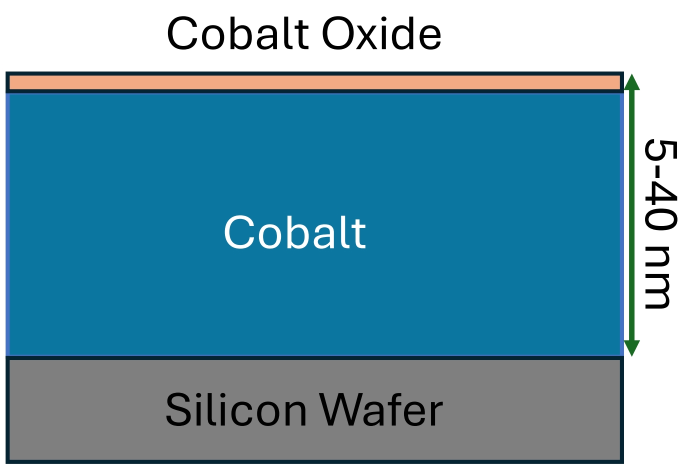

Figure 1.2 Schematic side view of the samples. A cobalt film is deposited on a silicon substrate. Because the cobalt layer is uncapped, a surface layer of cobalt oxide with an unknown thickness, likely no more than 1-2 nm, is expected to form. The thickness of the cobalt ranges from 5 to 40 nm.

1.2 Project Objective

The objective of this study is to characterize the magnetic response of single-layer cobalt (Co) thin films as a function of both applied magnetic field and film thickness. Specifically, we aim to determine how the out-of-plane (OOP) magnetic texture develops in simple thin-film systems and how its formation is influenced by thickness and external field conditions. To address this question, we examine films with the structure shown in Fig. 1.2 using Magnetic Force Microscopy (MFM) to resolve magnetic texture and Vibrating Sample Magnetometry (VSM) to obtain magnetization loops. By correlating the results from these two techniques, we seek to develop a more comprehensive understanding of the magnetic behavior in single-layer Co films, which may also provide insight into domain formation mechanisms in multilayer systems such as Co/Pt and Co/Au that are widely used in magnetic storage applications.

In this work, six samples with Co thicknesses ranging from 5 to 40 nm were investigated. Each sample consists of an uncapped cobalt film deposited on a silicon substrate. Due to the absence of a capping layer, a thin surface oxide layer—likely no more than 1–2 nm—is expected to form, as illustrated in Fig. 1.2. The substrates measure approximately 5 × 5 mm and contain a 100×100 μm observation window. The experimental procedures used for these samples are described in Chapter 2, and the resulting magnetic textures and their correlations with magnetization behavior are presented in Chapter 3.

Chapter 2

Methods

The process for measuring magnetic images via Magnetic Force Microscopy (MFM) is explained step-by-step. The method of obtaining magnetization loops via VSM is also described in detail.

2.1 VSM Technique

The Vibrating Sample Magnetometer (VSM) we use is part of the Physical Property Measurement System (PPMS) . This is a large vacuum chamber that allows for installing measurement tools as well as a cryostat used for cooling the samples with either liquid nitrogen and liquid helium, as well as a superconducting magnet, capable of producing magnetic fields up to 9 T.

In order to set up the VSM, we need to first insert a magnetic coilset into the vacuum chamber. The coilset is used to detect the magnetization in the material through the Faraday effect while a magnetic field is applied via the superconducting magnet. The next element inserted is a long tube with several rings and a rubber O-ring at the top of it. This is used as a guide for the sample to ensure that it makes it into the pickup coil. Finally, the VSM motor is placed on top of the sample holder to allow sample vibration inside the detection coil. The sample is then mounted as shown in

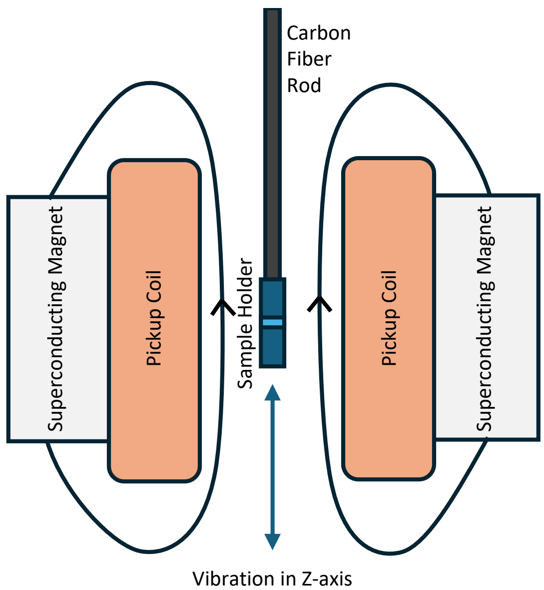

Figure 2.1 Depiction of the VSM instrument. A sample is placed such that it is either perpendicular or parallel to the applied field for OOP and IP measurements, respectively. Lines exiting the superconducting magnets represent the magnetic field. The superconducting magnet is computer-controlled and produces fields ranging from -9 T to 9 T. The pickup coil enables the determination of magnetization via the Faraday effect.

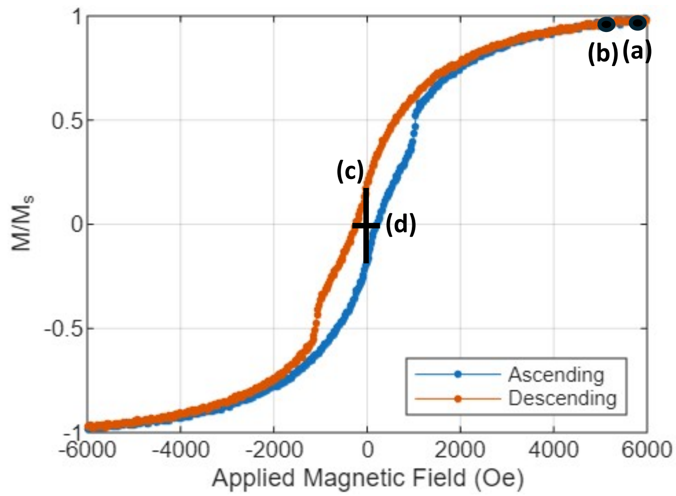

Figure 2.2 Major magnetization loop for the Co 40 nm sample and associated features. This loop was run from -10000 Oe to 10000 Oe, and we have chosen to show only -6000 Oe to 6000 Oe for illustrative purposes. The blue is the ascending branch, and the orange is the descending branch. (a) The nearly saturation point $H_s(98\%)$, which we deemed as when the sample reaches 98% of the highest magnetization at 10,000 Oe, where $H_s(98\%)$ is 6200 Oe. (b) The nucleation point H_n was measured by taking the derivative of the graph, resulting in $H_n = 5600$ Oe. (c) Remanent magnetization is measured as the difference in spacing between the two opposite intercepts at H = 0. The value is $M_r/M_s = 0.18$. (d) Coercivity H_c which is the difference between the two intercepts at M = 0 on the ascending and descending branches; in this case, H_c = 220 Oe.

Fig. 2.1 and is placed either perpendicular to the field for OOP measurements or parallel to the field for IP measurements.

The system is now ready to take data. At this point, we measure the magnetic loops by applying a magnetic field and detecting the resulting magnetization. For most of the magnetic loops taken, the range was -10000 Oe to 10000 Oe, and for the minor loops, they were typically started at -10000 Oe, and then a loop was run from 0 Oe to some number less than 10000 Oe. The data for magnetization loops is typically collected while sweeping the magnetic field in steps of 10 to 20 Oe. Different data points can be extracted from these loops as shown in Fig. 2.2.

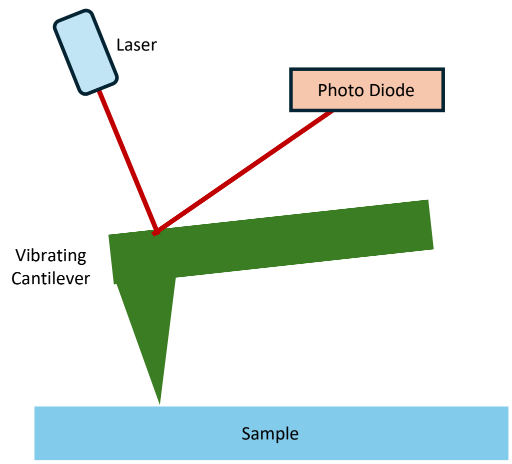

Figure 2.3 Depiction of the AFM technique: A vibrating cantilever taps the surface of the sample. Use of a laser and photodiode allows for determining the height of features on the sample.

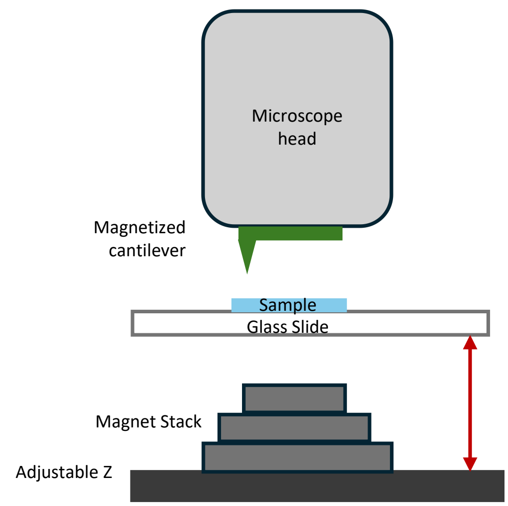

Figure 2.4 Schematics: Modifications made for MFM in-situ measurements. These include a glass slide extended over a magnet stack attached to an adjustable stage in the z direction.

2.2 AFM/MFM Techniques

Atomic Force Microscopy is a technique capable of resolving surface features at the nanoscale. This is possible using a tip that consists of a microscopic cantilever (Fig 2.3), which is vibrated, causing the tip to go up and down, and is positioned such that at the bottom of these vibrations the tip touches the sample, resulting in tapping. A laser is pointed at the tip of the cantilever, and the amplitude and phase change as the tip taps the surface. Based on this signal feedback, we can trace out a section of the sample and determine the physical height of the sample. We repeat this process until we have mapped out a square area of typical size 10 μm by 10 μm composed of a 512 x 512 pixel image.

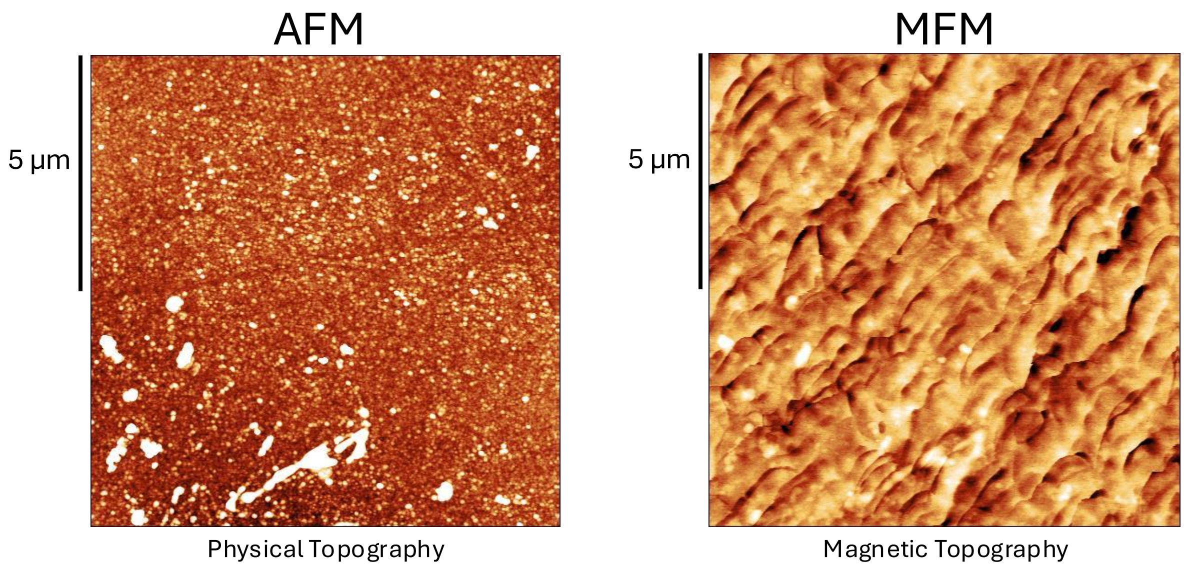

Figure 2.5 Example of difference in AFM and MFM imaging on the Co 15 nm sample at 1800 Oe. The image on the left shows an AFM image depicting the physical features of the sample. The image on the right is the magnetic topography as a result of the MFM process. Due to imperfections in the method, there is some amount of the AFM image present in the MFM image.

To visualize the magnetic texture at the surface, we begin by first performing regular AFM. After each line is traced out on the AFM, the tip is lifted and retraces the same path; we retrieve the MFM signal in arbitrary phase units. In order to detect the magnetic field, we use a cantilever that is coated with a very thin magnetic layer (typically of CoCr). The local magnetic moment existing at the end of the tip is then subject to a magnetic interaction with the magnetic field gradient emanating from the sample. After tracing out the surface topology via AFM of one line. The tip is raised to a certain lift height, typically between 20 nm and 100 nm above the surface of the sample, and traced back following the same topography. The phase difference between this image and the previous one shows the magnetic response, such as in Fig. 2.5

Taking in-situ MFM images is challenging, and as such, we follow a procedure. A simplified version is presented here; a more detailed version is shown in the appendix. We begin by turning on the machine and moving the stage, and attaching a magnet stage as shown in Fig. 2.4. In order to know what the applied field is for any particular measurement, we must calibrate the z-stage using a Hall sensor. We do this by first picking out a set of target magnetic field values, which, with our setup, is limited to the range of 0 Oe to 4000 Oe. The z-stage is translated up and down until the target field is reached, where we then note the readout on the z-stage in a notebook. We now set up the AFM as per standard, which includes placing the sample on the stage, magnetizing and mounting the AFM tip, and calibrating the tip. After this is complete, we engage the tip at the first target field with a scan frequency of 1.02 Hz and allow it to trace out the entire image, typically taking about 20 minutes. The resultant image(s) are flattened and exported, upon which the tip is disengaged, the z-stage is moved to the next target field value, and the tip is engaged again. This process is repeated until all target field values have been reached.

2.3 Image Processing

This section describes the image–analysis procedures applied to fully processed and flattened MFM images. Each method is used to extract quantitative information about magnetic domain structure and spatial organization.

2.3.1 Binarization

Binarization converts an image into a two–level representation in which each pixel is assigned either black or white. For Co/Pt multilayer samples, this approach has historically been effective because the domain morphology is relatively simple, enabling straightforward domain counting and facilitating Fourier–space analysis. In contrast, for single–layer cobalt films, the increased complexity of the domain structure makes binarization less reliable, often obscuring fine features rather than clarifying them. Examples of binarization are included in Fig. 2.6

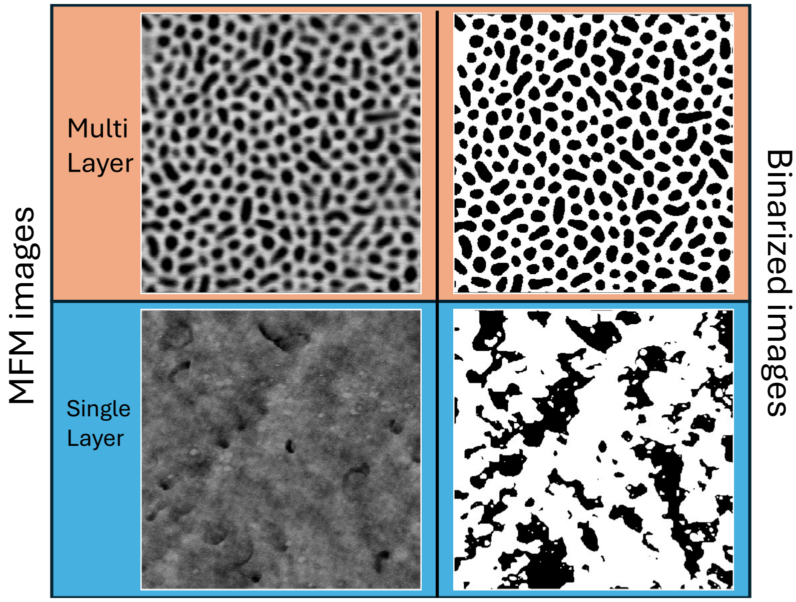

Figure 2.6 Illustration of the binarization process applied to MFM images. The top row shows a multilayer sample, where binarization produces a clear domain pattern. The bottom row shows a single–layer cobalt sample, where the same procedure yields a less interpretable result due to the more complex domain structure.

2.3.2 Wave Detection

Wave detection aims to identify the peaks of periodic magnetic features. This is accomplished using MATLAB's `edge` function with the Canny method. The algorithm is executed over a range of threshold values, and the resulting edge maps are combined with a weighting scheme that emphasizes features consistently detected at narrower thresholds. The final mask highlights the most robust wave–like structures in the image.

2.3.3 Density Counts

Quantifying the density of magnetic domains or wave features is essential for characterizing how magnetic texture evolves under varying applied fields. To perform this measurement, a binarized image is first generated using either the binarization method or the edge–based approach described above. MATLAB's `bwconncomp` function is then used to identify connected white regions. The number of these regions serves as a proxy for domain or wave density.

2.3.4 Fourier Space

Additional structural information is obtained by analyzing the images in Fourier space. A two–dimensional Fourier transform is applied to each MFM image, after which the central peak is removed. The next–largest peak is then identified, and its radial distance and angular position relative to the center are recorded. The radial distance corresponds to the inverse spatial frequency; taking its reciprocal yields the real–space periodicity, interpreted as the average spacing between wave features.

Further structural information for the single-layer samples is extracted using a 2D radial Gaussian fit. Our model is a sum of rotated anisotropic Gaussian Curves. In this procedure, we take the general form of a 2D Gaussian curve and fit it to the intensity profile obtained from the 2D Fourier transform. The fitted curve provides several useful parameters: the peak position, which corresponds to the dominant spatial frequency; the amplitude, which reflects the strength of the periodic modulation; the ellipticity of the Gaussian, which shows the degree of anisotropy present; and the full width at half maximum (FWHM), which characterizes the spread of spatial frequencies contributing to the observed texture. The width of the Gaussian is particularly important, as it provides an estimate of the coherence or uniformity of the wave-like magnetic structures. A narrow width indicates a well-defined periodicity, whereas a broader width suggests a more disordered or heterogeneous magnetic texture.

Chapter 3

Results

This chapter presents the experimental results obtained from both vibrating sample magnetometry (VSM) and magnetic force microscopy (MFM). The first section summarizes the magnetization loops and extracted magnetic parameters for each sample, while the second section provides representative MFM images accompanied by brief qualitative observations.

3.1 VSM Results

Using VSM, magnetization loops were measured for all six cobalt samples. Measurements were performed for both in-plane (IP) and out-of-plane (OOP) field orientations, as shown in Fig. 3.1.

For the thinnest sample (5 nm), shown in Fig. 3.1a, both IP and OOP magnetization curves exhibit minimal hysteresis, consistent with expectations for ultrathin cobalt films. As thickness increases, the OOP hysteresis becomes more pronounced, with the 40 nm sample (Fig. 3.1f) showing a noticeably larger hysteresis on the OOP loop. This trend aligns with the increasing contribution of perpendicular magnetic anisotropy in thicker films.

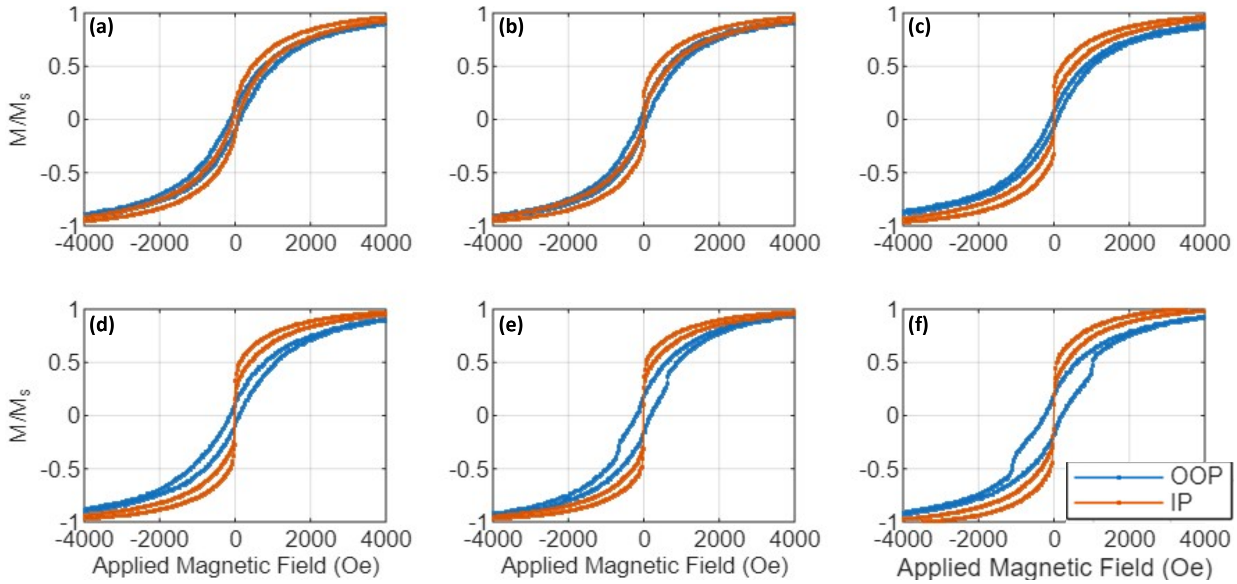

Figure 3.1 Magnetization loops for cobalt films of thickness (a) 5 nm, (b) 10 nm, (c) 15 nm, (d) 20 nm, (e) 30 nm, and (f) 40 nm. Each plot shows both the OOP and IP magnetization components. The displayed field range is -4000 to 4000 Oe, representing a zoomed-in portion of the full -10000 to 10000 Oe sweep.

We next extract quantitative magnetic parameters from each magnetization loop. Following the procedure illustrated in Fig. 2.2, we determine the saturation field, coercivity, nucleation field, and remanent magnetization. A MATLAB script performs this analysis for every recorded loop, and the resulting values are summarized in Fig. 3.2.

Figure 3.2a shows that the IP saturation field decreases monotonically with thickness, whereas the OOP saturation field initially increases, reaches a local minimum at 20 nm, rises again at 30 nm, and then decreases at 40 nm. The coercivity H_c (Fig. 3.2b) decreases with thickness up to 15 nm, after which the OOP coercivity begins a steady increase while the IP coercivity continues to decay exponentially. The nucleation field H_n (Fig. 3.2c) exhibits a similar trend to the saturation field, except that the OOP component shows a maximum at 20 nm rather than a minimum.

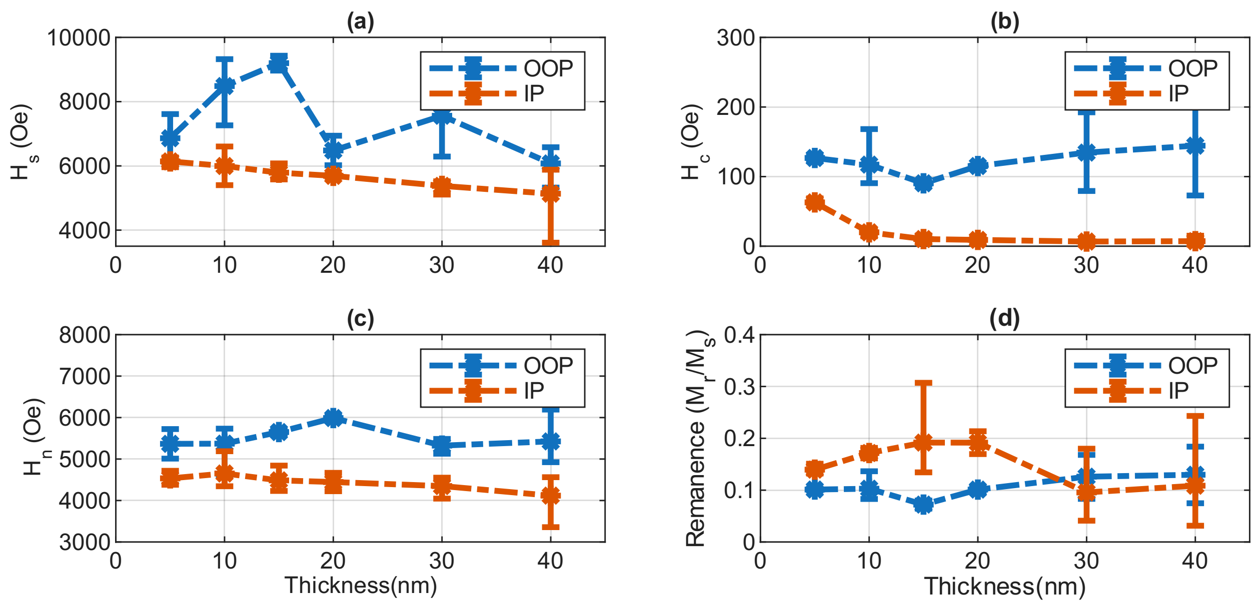

Figure 3.2 Magnetic parameters extracted from major loops as a function of cobalt thickness. Error bars represent the full range (minimum to maximum) of values obtained at each thickness, and the central point denotes the average. Shown are (a) saturation field H_s, (b) coercivity H_c, (c) nucleation field H_n, and (d) remanent magnetization M_r Normalized by M_s.

3.2 MFM Results

In this section, we show several images obtained via magnetic force microscopy (MFM) and describe the texture present. Images were acquired from each of the six Co thin-film samples. Following the imaging approach illustrated in Fig. 2.5, multiple MFM images are presented alongside an atomic force microscopy (AFM) image of the corresponding region. The AFM images remained unchanged throughout the imaging sequence and therefore provide a reference for the physical surface morphology, allowing magnetic contrast observed in the MFM images to be distinguished from topographic features.

For each sample, a sequence of MFM images is presented at selected applied magnetic field values. The selected fields include 0, 600, 900, 1200, 1500, 1800, 2100, 2700, and 3900 Oe, as well as the highest field at which an image was acquired. Greater emphasis is placed on the lower-field images because, as discussed in the following sections, the most significant changes in the magnetic texture generally occur at relatively low applied fields. The images are examined qualitatively with particular attention given to the evolution of magnetic domain morphology, contrast, characteristic length scales, and apparent anisotropy as a function of applied field.

Unless otherwise stated, all MFM and AFM images cover a 10 μm $\times$ 10 μm region and were acquired using Bruker MESP-V2 HM magnetic force microscopy tips. The MFM measurements were performed while varying the applied magnetic field, allowing the evolution of the magnetic texture to be observed throughout the magnetization process.

3.2.1 5 nm Sample

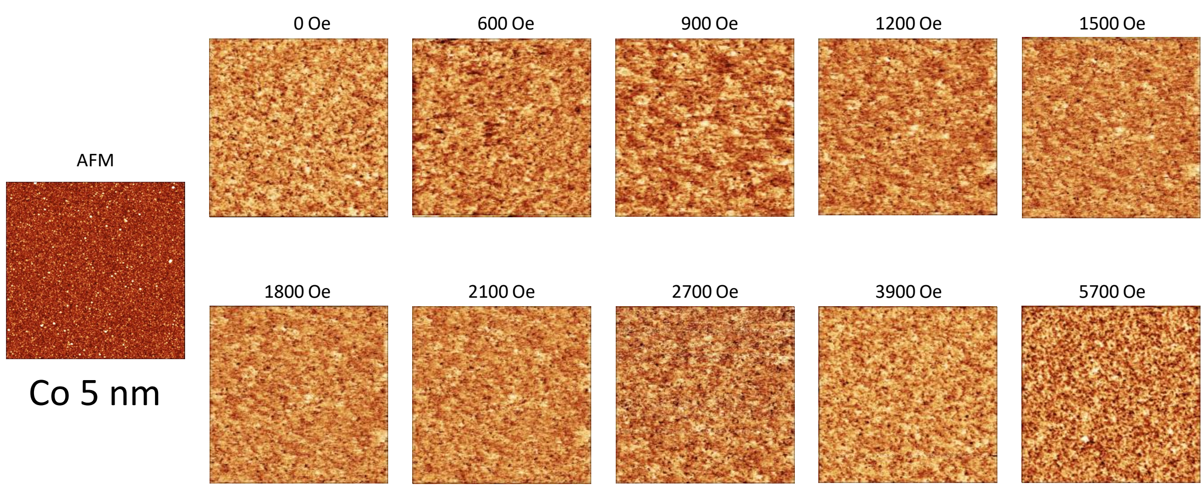

Figure 3.3 MFM and AFM images for the 5 nm sample. The applied magnetic field was varied from 0 to 5700 Oe.

The 5 nm Co film contains the smallest amount of magnetic material among the samples investigated and consequently exhibits the weakest and least clearly resolved magnetic contrast. The MFM images from this sample are characterized by relatively high levels of granular background contrast and contain numerous small-scale features that change between successive applied-field values. These features are substantially less well defined than those observed in the thicker Co films, making it difficult to identify individual magnetic domains or domain structures with confidence.

The observed contrast in this sample is potentially disturbed by the presence of a cobalt oxide (CoO) layer of unknown thickness at the surface. Because the Co layer is not capped, oxidation of the surface is expected, and the relative contributions of the Co and CoO layers to the measured magnetic signal cannot be determined directly from these measurements. In addition, the AFM measurements indicate a height variation of approximately 10 nm across the imaged region. This relatively large topographic variation may contribute to the observed MFM contrast, further complicating the separation of magnetic and topographic effects. Consequently, while the MFM images indicate field-dependent contrast, the magnetic origin of the smallest features in this sample cannot be established unambiguously.

3.2.2 10 nm Sample

The 10 nm Co sample contains approximately twice the thickness of magnetic material as the 5 nm sample. However, the relative contributions of the Co film, the surface oxide layer, and the underlying Si substrate to the measured signal remain difficult to determine quantitatively. Despite this uncertainty, the MFM images exhibit substantially improved contrast compared with the 5 nm sample. The images are less granular and display magnetic structures that are more readily distinguished from the underlying physical surface morphology.

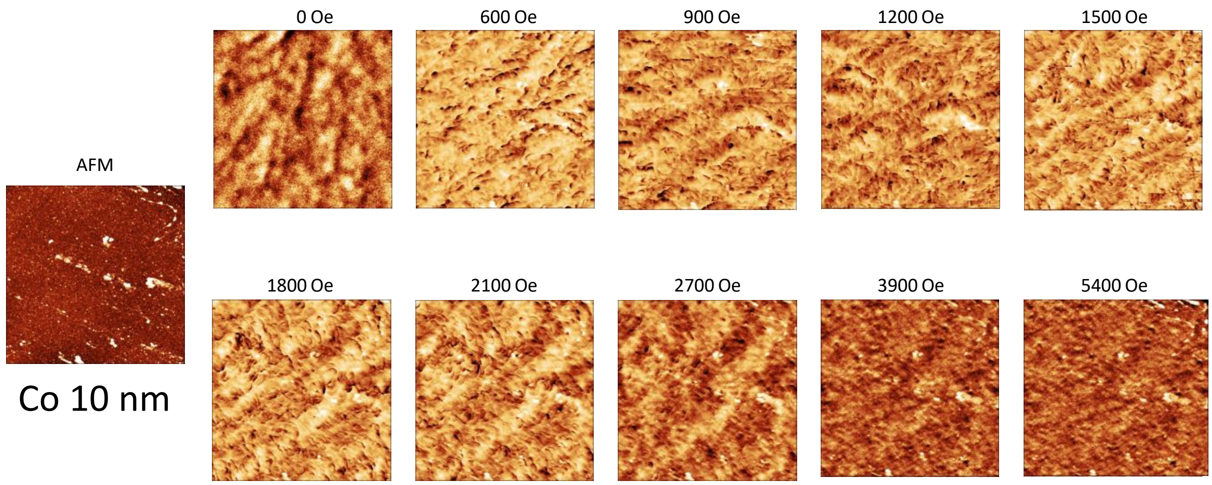

Figure 3.4 MFM and AFM images for the 10 nm sample. The applied magnetic field was varied from 600 to 5400 Oe on the ascending branch. The image at 0 Oe corresponds to a 5 μm image acquired at remanence and is included to provide continuity with the subsequent measurements.

As shown in Fig. 3.4, the MFM image at 600 Oe contains numerous small, crescent-shaped or wave-like regions of magnetic contrast with relatively weak directional preference. As the applied magnetic field is increased, these structures undergo substantial changes in their size, position, and orientation. Individual features appear to move and rotate between successive measurements, while new structures emerge and existing structures diminish. The broad background contrast also decreases progressively with increasing field.

A notable characteristic of the 10 nm sample is the large number of magnetic features and their pronounced sensitivity to the applied magnetic field. At relatively low fields, the wave-like structures become increasingly prominent as the field is increased. The number and apparent density of these features reach a maximum at approximately 2000 Oe, beyond which the contrast associated with the structures decreases rapidly. At higher fields, the wave-like features progressively merge into the background and become difficult to distinguish as the sample approaches magnetic saturation. This behavior suggests that a substantial portion of the magnetic reconfiguration in the 10 nm sample occurs over a relatively narrow range of applied fields.

3.2.3 15 nm Sample

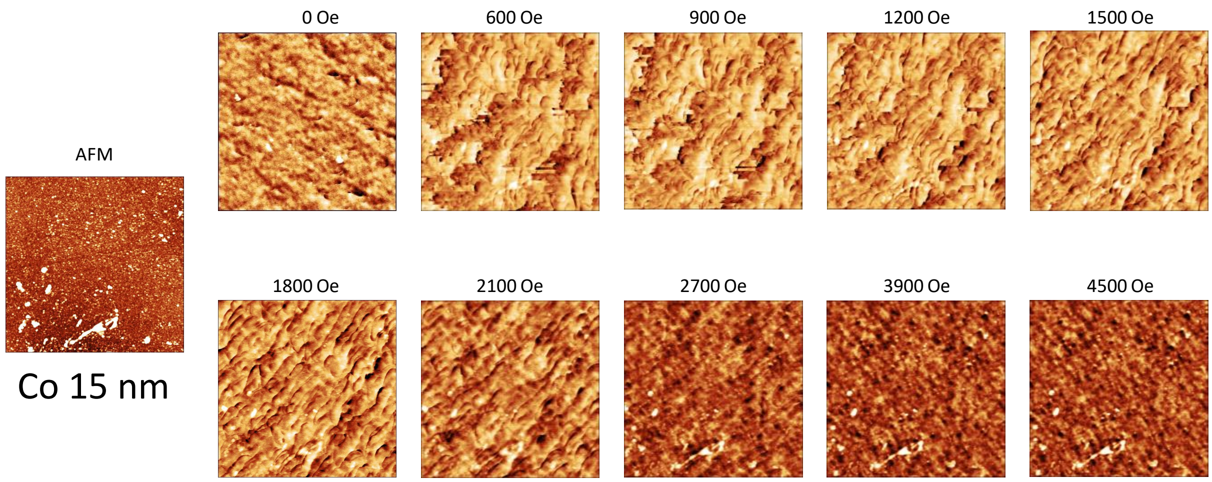

Figure 3.5 MFM and AFM images for the 15 nm sample. The applied magnetic field was varied from 0 to 4500 Oe on the ascending branch.

For the 15 nm Co film, the increased amount of magnetic material produces more clearly resolved magnetic contrast, providing greater confidence that the observed features originate primarily from the Co layer. At 0 Oe, several wave-like magnetic structures are already visible in the MFM image, indicating that a nonuniform magnetic configuration remains at remanence. As the applied magnetic field is increased, these regions of magnetic contrast become more pronounced and appear to expand, with additional smaller structures developing in their vicinity.

This evolution continues through approximately 2100 Oe, at which point the magnetic contrast begins to decrease substantially. With further increases in the applied field, the domain structures progressively disappear, leaving a relatively uniform background contrast. This transition is consistent with the sample approaching a more uniformly magnetized state at high applied fields.

Another notable characteristic of the 15 nm sample is the presence of a preferred direction in plane, for the formation of magnetic textures. At lower fields, the wave-like structures exhibit apparent anisotropy oriented from the bottom-left toward the top-right of the images. As the applied magnetic field increases, this preferred direction rotates slightly in the clockwise direction.

3.2.4 20 nm Sample

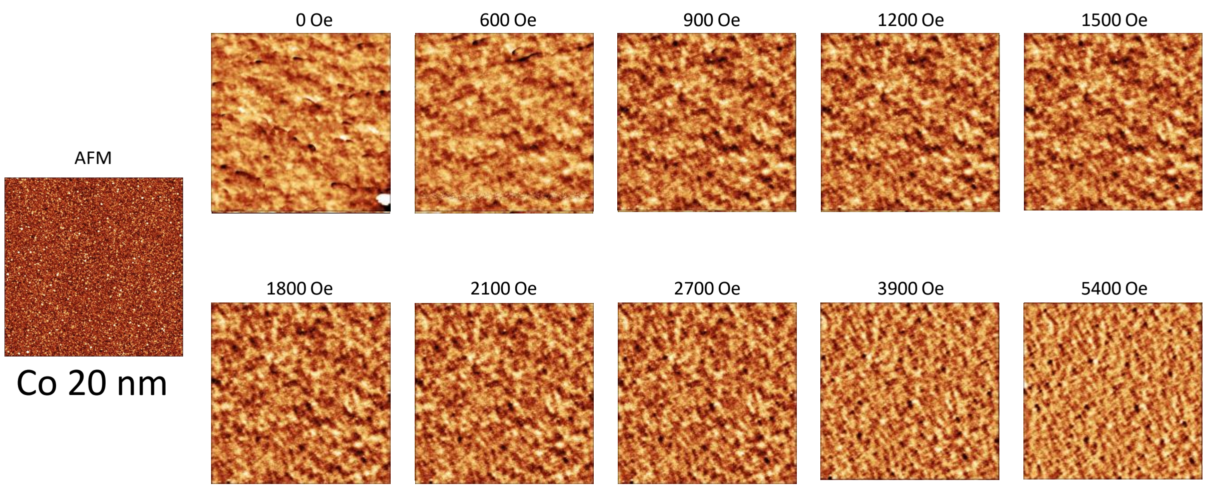

Figure 3.6 MFM and AFM images for the 20 nm sample. The applied magnetic field was varied from 0 to 5400 Oe on the ascending branch.

The MFM images obtained from the 20 nm Co film exhibit a substantial change in magnetic morphology compared with the 15 nm sample. Despite the relatively small increase in Co thickness, the wave-like magnetic structures that are prominent in the 15 nm sample are largely absent. Instead, the MFM images are dominated by diffuse regions of contrast and localized features resembling shallow divots or depressions in the magnetic signal.

These features gradually change in appearance and contrast as the applied magnetic field is increased. In particular, the background contrast becomes progressively more uniform, while local features shift and diminish. Only a relatively small number of distinct wave-like structures can be identified throughout the field sequence. The relatively weak and diffuse nature of the magnetic contrast makes the domain morphology of this sample less readily identifiable than that of the 10 nm and 15 nm samples.

The change in morphology between the 15 nm and 20 nm samples demonstrates that the magnetic texture does not evolve monotonically with Co thickness. Instead, relatively small changes in film thickness can produce significant differences in the observed domain structure. This observation motivates a more detailed comparison of the magnetic textures and their characteristic length scales across the full range of sample thicknesses.

3.2.5 30 nm Sample

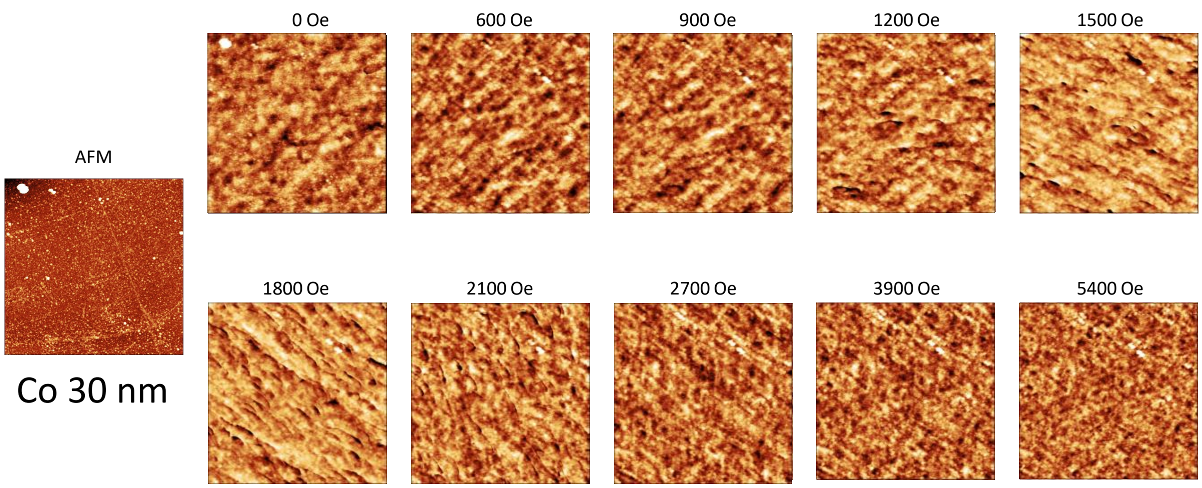

Figure 3.7 MFM and AFM images for the 30 nm sample. The applied magnetic field was varied from 0 to 5400 Oe on the ascending branch.

The 30 nm Co sample contains substantially more magnetic material than the 20 nm sample. Based on the behavior observed in the thinner samples, one might expect the wave-like magnetic structures to become less prominent with increasing Co thickness. The initial low-field images are consistent with this expectation, as relatively few well-defined magnetic features are observed. However, as the applied field is increased, wave-like structures begin to emerge, becoming increasingly distinct between approximately 900 and 1500 Oe.

The wave-like structures are most clearly visible at intermediate field values before gradually diminishing as the applied field is increased further. At higher fields, the magnetic contrast becomes comparatively uniform, with relatively little discernible domain structure. The disappearance of the wave-like features is therefore accompanied by a reduction in the spatial variation of the MFM signal, consistent with the sample approaching a more uniformly magnetized state.

The magnetic texture also exhibits some in-plane anisotropy. At approximately 1200 Oe, the structures display a preferred orientation that is approximately horizontal, extending predominantly from left to right. With increasing applied field, this preferred direction changes substantially. By approximately 2100 Oe, the apparent anisotropy has rotated by roughly 90°, resulting in a predominantly vertical orientation. As the wave-like structures subsequently disappear at higher fields, the apparent anisotropy also becomes less pronounced. This correlation suggests that the observed directional preference is closely associated with the presence and morphology of the wave-like magnetic domains.

3.2.6 40 nm Sample

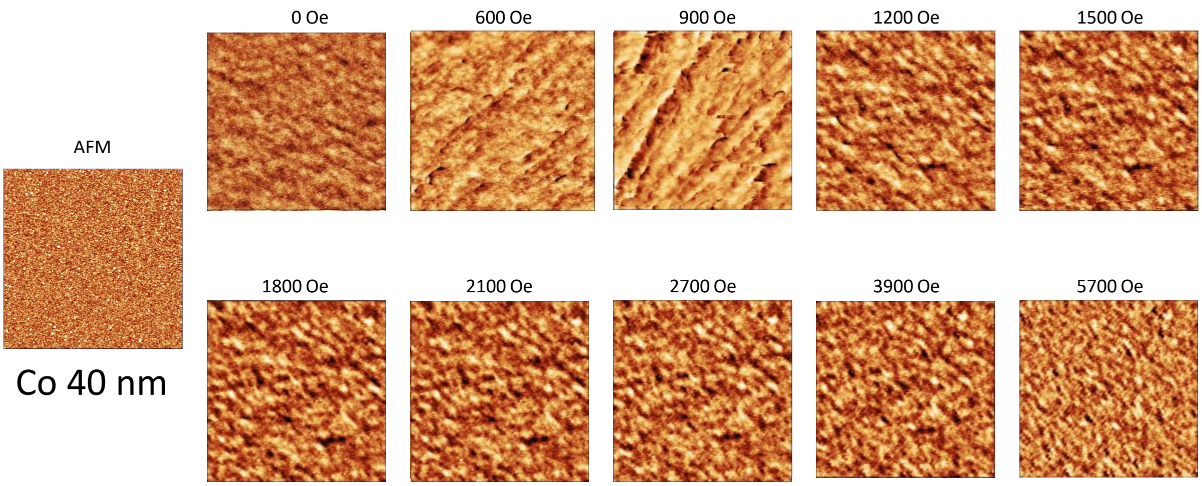

Figure 3.8 MFM and AFM images for the 40 nm sample. The applied magnetic field was varied from 0 to 5700 Oe on the descending branch. The AFM image corresponds to the 800 Oe MFM scan.

The 40 nm Co film represents the thickest sample investigated in this study. Based on the behavior observed in the thinner films, one might expect the onset of the wave-like magnetic structures to occur at progressively higher applied fields as the Co thickness increases. However, the 40 nm sample does not follow this trend. As shown in Fig. 3.8, wave-like magnetic structures are already apparent at approximately 600 Oe and become most prominent near 900 Oe before rapidly decreasing in contrast at higher fields.

Following the disappearance of these textures, the MFM images become comparatively uniform at high applied fields. In particular, there is little apparent change between the 3900 Oe and 5700 Oe images despite the substantial increase in applied field. This suggests that the magnetic configuration has become relatively stable over this portion of the field range and may indicate that the sample is approaching saturation.

The 40 nm sample also exhibits a pronounced change in the in-plane directivity of the magnetic texture. At approximately 900 Oe, the wave-like structures display a preferred orientation extending from the bottom-left toward the top-right of the image. This orientation changes substantially between 900 and 1200 Oe. By 1200 Oe, the preferred direction appears to have rotated such that the structures extend approximately from the top-left toward the bottom-right. The rapid change in orientation over this relatively small range of applied field indicates that the magnetic texture is highly field-dependent in this regime.

Overall, the 40 nm sample demonstrates that increasing the Co thickness does not simply result in a systematic shift of the magnetic texture toward higher applied fields. Instead, the onset, morphology, and anisotropy of the observed magnetic structures vary nonlinearly with thickness. These observations provide motivation for comparing the MFM results across all six samples in order to identify trends in the field-dependent magnetic behavior.

3.3 Analysis in Real Space

In this section, we perform an analysis on the mfm images in real space via MATLAB and manual counting.

3.3.1 Manual Counting

Using the dataset taken from the most recent HM tip series on the Bruker AFM, we painstakingly counted out every wave, tracing a line end to end and measuring that length. Taking the result and interpolating it between each of the samples results in Fig. 3.9.

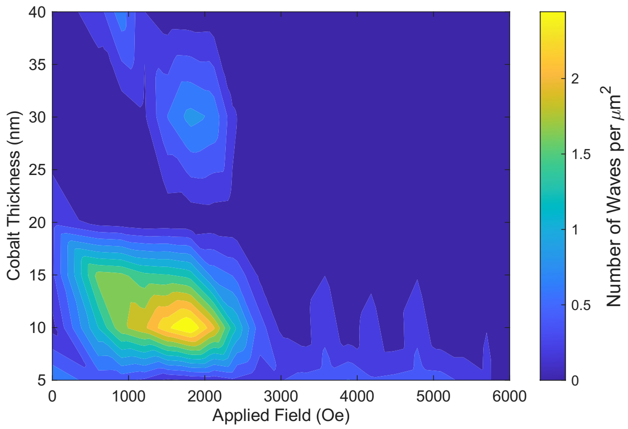

Figure 3.9 Manually measured wave density (in waves per μm^2) is shown. Counts were done by tracing out lines on top of the image from one end to the next. Each of these was then counted, resulting in the graph shown, which is a lower-bound estimate of the true values.

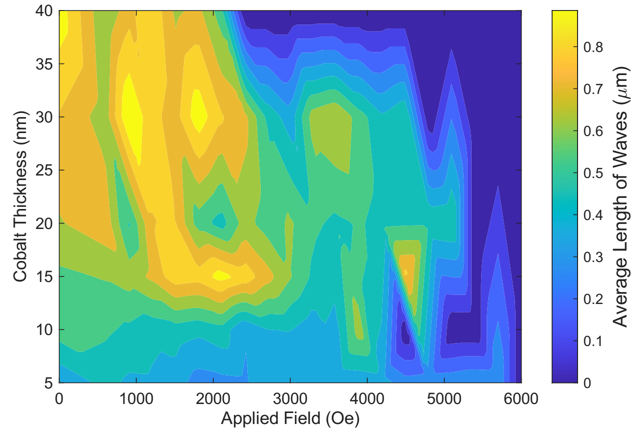

Figure 3.10 The average length of the wave-like structures in μm. These were found by averaging the length taken from end to end of each of the waves. Since the distance was counted end to end, this is a lower-bound of the true values.

3.3.2 Wave Densities and Directivity

Similar to how we have done an analysis by manually counting waves, we do something similar in MATLAB following the procedure outlined in the Section on Wave Detection. This method works well when there are strong waves found across the image; however, in the case that the waves are either small, low contrast, or nonexistent, the program will find a large number of waves that are not real. This causes the program to create a graph that is nearly the exact inverse of that found by manually counting each of the waves. Further work utilizing machine learning to accurately count the number of waves present would be a great next step for a future student in our group.

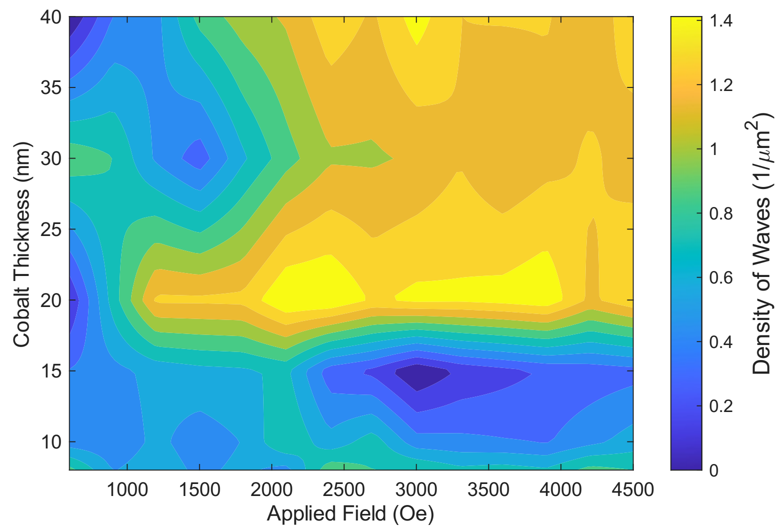

Figure 3.11 Wave density as determined via MATLAB. This value should be taken as an underestimate at values where wave texture is seen, and an overestimate at values where the texture is gone.

3.4 Analysis in Fourier space

3.4.1 Gaussian Fits

Using the instructions in the methods section, we analyze each image by first removing its average value. Then taking the 2D Fourier transform and fit a 2D Gaussian curve. The values of note that we keep are the full width at half maximum (FWHM) and the curve's ellipticity. The FWHM represents the distance between features on the MFM images. The ellipticity is a measure of how much like an ellipse the 2D Gaussian is, showing us the strength of any existing anisotropy . These graphs may be best understood as representing the anisotropy and distance between magnetic textures that are not necessarily wave patterns.

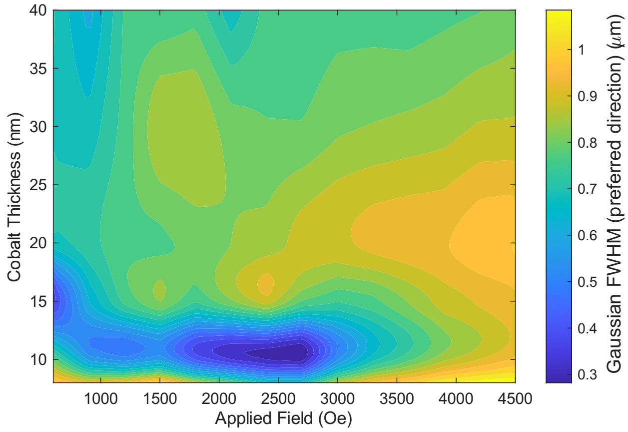

Figure 3.12 Full width at half max for Gaussians in the preferred direction.

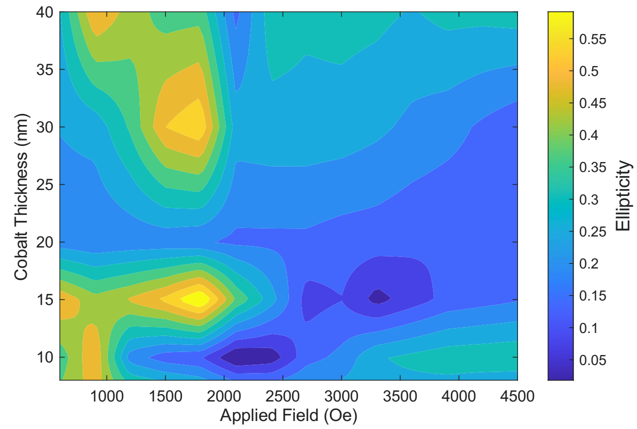

Figure 3.13 Ellipticity of the Gaussian, which details how much, if any, anisotropy is present.

Chapter 4

Discussion

This chapter presents an interpretation of the experimental results as well as the overall conclusions of the study.

4.1 Interpretation

4.1.1 Domain Walls

The wave-like structures observed in the MFM images are most plausibly attributed to the out-of-plane magnetization components arising at the domain walls between domains of predominantly in-plan magnetization. The gradual rotation of the magnetization at the domain walls may follow either Bloch or Néel types. The formation of these walls can be understood by considering the underlying domain structure of the cobalt films. The domains themselves are predominantly in-plane, but the transition regions (domain walls) between adjacent domains contain localized out-of-plane magnetization, producing the wave-like contrast in MFM.

This interpretation is consistent with the disappearance of the wave-like texture under increasing magnetic field. As the external field strengthens, domain walls widen, and the magnetization becomes more uniformly aligned, thereby reducing the out-of-plane features responsible for the observed waves. Representative domain structures are shown in Fig. 4.1.

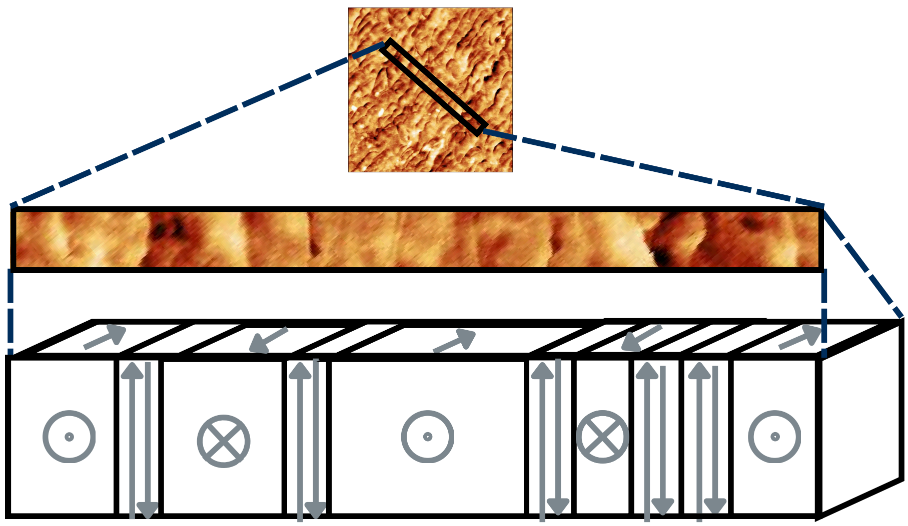

Figure 4.1 Depiction of magnetic texture formation. Arrows represent the directions of local magnetization domains.

4.1.2 Wave Density as a Function of Thickness

The increased density of wave-like features in thinner samples can be rationalized by examining the in-plane and out-of-plane magnetization loops shown in Fig. 3.1. As film thickness decreases, the IP and OOP hysteresis loops become increasingly similar. This suggests that the energetic cost of forming out-of-plane domain-wall structures is reduced in thinner films, making the wave-like texture more favorable.

From the collected data, several trends emerge. At medium field values, samples tend to exhibit a substantial density of wave-like features. This relationship indicates that the onset of smooth magnetization behavior may serve as a predictor for the presence of significant texture.

4.1.3 Connection Between Magnetization Loops and Texture

Establishing a direct relationship between the MFM-imaged texture and the VSM magnetization loops has proven challenging. Nevertheless, Fig. 4.2 reveals partial correlations for several thicknesses, particularly in panels (b), (c), (e), and (f). In these cases, the number of waves decreases markedly once the out-of-plane magnetization exceeds roughly 60% of the saturation value.

In contrast, samples with thicknesses of 5 nm and 20 nm (Fig. 4.2(a,d)) do not exhibit a clear correspondence between texture evolution and magnetization behavior. These deviations highlight the complexity of domain-wall formation and the sensitivity of thin-film magnetic textures to local sample conditions.

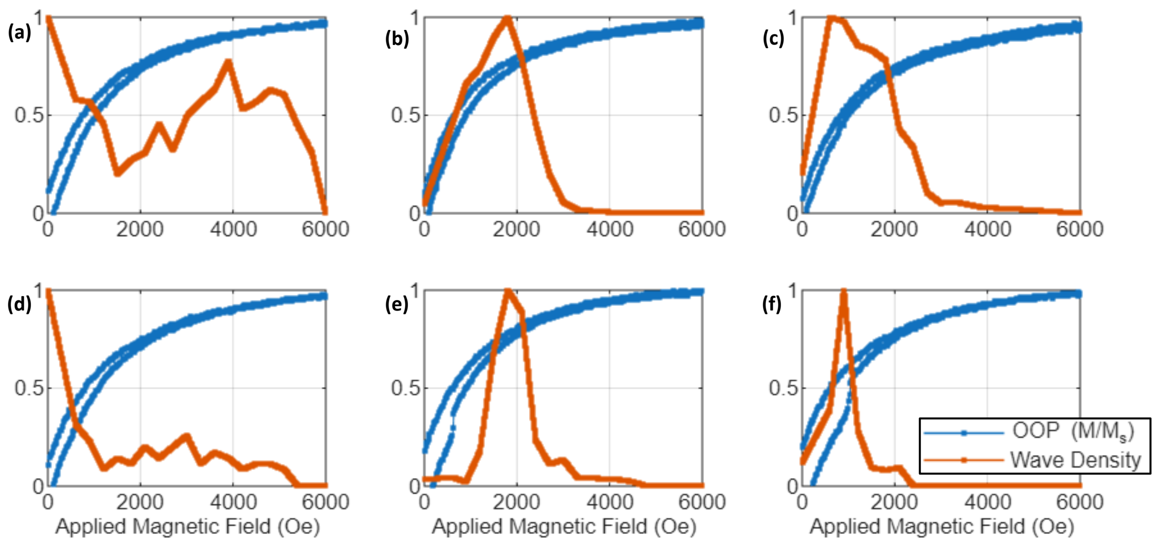

Figure 4.2 Wave density present in the texture plotted against the respective magnetization loop for each cobalt thickness: (a) 5 nm, (b) 10 nm, (c) 15 nm, (d) 20 nm, (e) 30 nm, and (f) 40 nm. Each plot shows the out-of-plane magnetization (OOP) as well as the normalized number of waves.

4.2 Conclusion

In this project, we aimed to determine how the OOP magnetic texture develops in simple ferromagnetic thin-film systems and how its formation is influenced by thickness and external field. For single-layer Co films, we observe a distinct transformation in magnetic texture under an external field. The wave-like texture dominant at low fields diminishes at field values (about 2000 Oe) much lower than saturation field values (about 8000 Oe). This texture exhibits a preferred orientation that shifts under applied field, and its density is not maximized at remanence but instead at intermediate field values. These findings suggest that the formation and stability of wave-like features are governed more strongly by field magnitude and local sample morphology than by hysteresis alone.

Several limitations should be noted. MFM measurements are highly sensitive to day-to-day variations in both instrument performance and sample conditions, which can affect reproducibility. For this thesis, representative datasets were selected to best reflect the overall trends observed across multiple measurements.

Future work could include independent verification of cobalt layer thicknesses, exploration of higher magnetic fields to assess their influence on texture hysteresis, and comparative studies between single-layer and multilayer films to determine interlayer coupling effects on domain-wall formation and magnetic texture. We have established that nanoscale magnetic textures present in single-layer Co evolve and decay based on external magnetic field strength. This texture and its evolution are dependent upon film thickness, where we have identified an optimal region for wave-like texture formation, located around 10-15 nm at field values of 1800-2100 Oe. Understanding the formation of these textures in single-layer films allows us to compare the evolution with that of more complex multilayer systems.

Appendix A

Veeco Dimension V AFM/MFM setup

Taking data as described in the AFM/MFM section above requires a certain amount of setup to occur first. Here we outline the necessary steps for the AFM we use, which are a VEECO Dimension V Atomic Force Microscope as well as a brand new Bruker Atomic Force Microscope. The process for using the VEECO AFM is given below. For the curious reader, the guide for using the new Bruker Atomic Force Microscope is provided in the Appendix under AFM SOP.

To begin using the AFM, we first turn on a constant power supply. The desktop capable of running the software is turned on while the power supplies connected to the AFM are turned on. Once the computer is up and running, we start the program and choose the workspace, which contains the settings for the run, and open Meter, Navigation, Dual-Scan, and Parameters windows.

Using the Navigation window, we move the Z motor such that the microscope head is as far away from the stage as possible. The X and Y motors are then used to translate the stage, leaving space for the in-situ modifications shown in Fig. 2.2

A set of clamps is used in concert with an aluminum block to attach the adjustable Z stage to the AFM. The stage includes a flat magnetic surface where a magnet stack of some size can be easily mounted. After mounting the magnets, we move them until the laser from the microscope head is pointed at the center of the magnet stack. The stage also has a knob. This knob measures the distance from the bottom of the stage to the bottom of the AFM table. Turning it clockwise causes the stage to rise, and similarly, the stage goes down if the knob is rotated counterclockwise.

Once the Z stage and magnet stack have been set up, we now move to calibrating the magnetic field. We do this via the use of a hall sensor probe. In order to mount the probe, we first need to mount a glass slide using a set of small permanent magnets to a steel block present on the AFM stage. We then place the probe in the groove present on the glass slide and move the glass slide until the laser from the microscope head is pointed at the tip of the probe. This process places the probe directly above the magnets.

The reading on the box is then compared to the predetermined field values for the day's experiment. The Z-stage is translated up and down until all field values have been reached and the values for the Z-stage have been noted. Once complete, the probe and box are dismounted, unplugged, and put away.

Once magnetic calibration has been completed, we mount the sample by placing it on the glass slide face up. If the calibration included high field values, we place the sample on a piece of double-sided tape so that it is unable to 'flip' under high field. An AFM tip is then chosen. The typical choice for these experiments has been a low-coercivity tip. The tip is magnetized and then mounted to the microscope head. Once mounted, the laser is moved such that it points at the tip of the tip, and a diffraction pattern is observed.

Using the computer, we first navigate to the Parameters window and switch the mode to Contact. Using the Meter window, we twist several knobs until the red dot is focused on the center within .05 mV. The mode is switched back to Tapping. We then use the z-motor until the tip is close enough to the surface that we can identify an edge of our sample. Using this edge as our guide, we continue using the z-motor until the image shown on the navigate screen is in focus.

With the sample in focus, we now wish to tune the sample. This is done by first clicking on the Scan-Dual window and then on the tuning fork in the upper menu. We set the range to be an appropriate one; for the LC tip, this is 10 kHz to 100 kHz, and press autotune. The resulting frequency is then typed into the drive frequency parameter on the Parameters window for both the Interleave and the AFM columns.

Interleave mode is now turned off, and we press the engage button. This brings the tip into contact with the sample. After contact is made, the Amplitude Setpoint is decreased by about 30 percent. Interleave mode is now switched to lift, and we watch a few lines, making adjustments to the parameters until the image is clear and in focus. Once complete, we set the direction to frame down and wait until the image is finished.

While the image is being taken, we navigate to the Realtime menu and change the Capture Filename. This allows us to determine the filename and directory of the data to be written. Having selected appropriate values and the image completed, we use the Capture Last button under Realtime. This takes the last full window of data, gives it the filename, and puts it in the assigned directory. The directory is navigated to in the program. Finding the newly taken image, we double-click on it and use the flatten tool to get an image from the raw data. This image is then exported using the export graphic command under the Files menu

Appendix B

Bruker AFM/MFM SOP

The most up to date AFM/MFM SOP can be found here

https://www.overleaf.com/read/rnvfxycbrdzh#2ed707

Bibliography

[1] "Fundamental Magnetization Processes in Thin-Film Recording Media," in *Solid State Physics* (Academic Press, 1992), Vol. 46, pp. 271–371, iSSN: 0081-1947.

[2] C. Chappert and P. Bruno, "Magnetic anisotropy in metallic ultrathin films and related experiments on cobalt films (invited)," Journal of Applied Physics **64,** 5736–5741 (1988).

[3] A. S. Westover, K. Chesnel, K. Hatch, P. Salter, and O. Hellwig, "Enhancement of magnetic domain topologies in Co/Pt thin films by fine tuning the magnetic field path throughout the hysteresis loop," Journal of Magnetism and Magnetic Materials **399,** 164–169 (2016).

[4] K. Chesnel *et al.*, "Morphological stripe-bubble transition in remanent magnetic domain patterns of Co/Pt multilayer films and its dependence on Co thickness," Physical Review B **98,** 224404 (2018), publisher: American Physical Society.

[5] W. Griggs, A. Peasey, F. Schedin, M. S. Anwar, B. Eggert, M. A. Mawass, F. Kronast, H. Wende, R. Bali, and T. Thomson, "Magnetic imaging of thermally switchable antiferromagnetic/ferromagnetic modulated thin films," Acta Materialia **283,** 120515 (2025).

[6] X. Z. Yu, N. Kanazawa, Y. Onose, K. Kimoto, W. Z. Zhang, S. Ishiwata, Y. Matsui, and Y. Tokura, "Near room-temperature formation of a skyrmion crystal in thin-films of the helimagnet FeGe," Nature Materials **10,** 106–109 (2011), publisher: Nature Publishing Group.

[7] A. Gentillon, C. Richards, L. A. Ortiz-Flores, J. Metzner, D. Montealegre, M. Healey, K. Cardon, A. Westover, O. Hellwig, and K. Chesnel, “Robustness of the remanent magnetic domain pattern formation and associated stripe-bubble transitions in Co/Pt multilayers against field sequencing,” AIP Advances **11,** 015339 (2021).

[8] L. Fallarino, A. Oelschlägel, J. A. Arregi, A. Bashkatov, F. Samad, B. Böhm, K. Chesnel, and O. Hellwig, “Control of domain structure and magnetization reversal in thick Co/Pt multilayers,” Physical Review B **99,** 024431 (2019), publisher: American Physical Society.

[9] H. W. Fuller and M. E. Hale, “Determination of Magnetization Distribution in Thin Films Using Electron Microscopy,” Journal of Applied Physics **31,** 238–248 (1960).

Index